Helix Switching of a Key Active-Site Residue in the Cytochrome *cbb*$_3$ Oxidases[†]

James Hemp,[‡,§] Caroline Christian,[‡] Blanca Barquera,[||,⊥] Robert B. Gennis,[‡,§,||] and Todd J. Martínez*[,‡,§]

Department of Chemistry, Department of Biochemistry, and Center for Biophysics and Computational Biology, University of Illinois, Urbana, Illinois 61801

Received March 14, 2005; Revised Manuscript Received June 20, 2005

ABSTRACT: In the respiratory chains of mitochondria and many aerobic prokaryotes, heme−copper oxidases are the terminal enzymes that couple the reduction of molecular oxygen to proton pumping, contributing to the protonmotive force. The *cbb*$_3$ oxidases belong to the superfamily of enzymes that includes all of the heme−copper oxidases. Sequence analysis indicates that the *cbb*$_3$ oxidases are missing an active-site tyrosine residue that is absolutely conserved in all other known heme−copper oxidases. In the other heme−copper oxidases, this tyrosine is known to be subject to an unusual post-translational modification and to play a critical role in the catalytic mechanism. The absence of this tyrosine in the *cbb*$_3$ oxidases raises the possibility that the *cbb*$_3$ oxidases utilize a different catalytic mechanism from that of the other members of the superfamily. Using homology modeling, quantum chemistry, and molecular dynamics, a model of the structure of subunit I of a *cbb*$_3$ oxidase (*Vibrio cholerae*) was constructed. The model predicts that a tyrosine residue structurally analogous to the active-site tyrosine in other oxidases is present in the *cbb*$_3$ oxidases but that the tyrosine originates from a different transmembrane helix within the protein. The predicted active-site tyrosine is conserved in the sequences of all of the known *cbb*$_3$ oxidases. Mutagenesis of the tyrosine to phenylalanine in the *V. cholerae* oxidase resulted in a fully assembled enzyme with nativelike structure but lacking catalytic activity. These findings strongly suggest that all of the heme−copper oxidases utilize the same catalytic mechanism and provide an unusual example in which a critical active-site residue originates from different places within the primary sequence for different members of the same superfamily.

Heme−copper oxidases are the terminal enzymes in the respiratory chains of mitochondria and many aerobic prokaryotes. These enzymes catalyze the reduction of molecular oxygen to water, coupling the redox free energy of the reaction to proton translocation across the membrane (*1*−*3*). Subunit I is the core of the enzyme complex containing all of the amino acid residues and cofactors (two hemes and a copper ion) necessary for both the reduction of O_2 to water and for the pumping of protons across the membrane. Subunit I of the heme−copper oxidases belongs to the heme−copper oxidase superfamily of enzymes, which also includes the integral membrane nitric oxide reductases. Oxidase members of the superfamily vary in the type of electron donor (cytochrome *c*, quinol, or high-potential iron−sulfur protein), the types of hemes (A, B, or O), and the number of subunits present in the enzymatic complex (ranging from 2, in some bacteria, to as many as 13 in mammalian mitochondria) (*4*, *5*).

Recent work on the evolutionary relationships of the heme−copper superfamily based on sequence alignments and structural information has identified three very distinct families (*6*). Members of the type A oxidase family are most similar to the *aa*$_3$-type oxidases from mitochondria. The type B oxidase family members are related to the *ba*$_3$-type oxidase from *Thermus thermophilus*. The type C oxidases are *cbb*$_3$-type oxidases, typified by the FixN enzyme from *Bradyrhizobium japonicum* (*7*). The type C oxidases have been speculated to be the most phylogenetically ancient, and their sequence similarities to the nitric oxide reductases (NORs)[1] have led to the idea that the respiratory oxidases were derived from enyzmes involved in denitrification (*8*, *9*).

X-ray crystal structures have been reported for members of both the type A and B families, providing a basis for the first theoretical studies of active-site chemistry in oxidases (*10*−*14*). Proteins with reported crystal structures include the mitochondrial cytochrome *c* oxidase from *Bos taurus* (*15*−*17*) (type A), the prokaryotic cytochrome *c* oxidases from *Paracoccus denitrificans* (*18*, *19*) (type A), *Rhodobacter sphaeroides* (*20*) (type A), and *Thermus thermophilus* (*21*) (type B), as well as the ubiquinol oxidase from *Escherichia coli* (*22*) (type A). In all of these enzymes, subunit I contains a six-coordinate low-spin heme, which accepts electrons from the electron donor, and a binuclear

[†] Support for this work was provided by the National Science Foundation (BES-04-03846 to T.J.M.) and the National Institutes of Health (to R.B.G.). T.J.M. is a Packard Fellow and a Dreyfus Teacher Scholar.

* To whom correspondence should be addressed. Telephone: (217) 333-1449. Fax: (217) 244-3186. E-mail: tjm@spawn.scs.uiuc.edu.

[‡] Department of Chemistry.

[§] Center for Biophysics and Computational Biology.

[||] Department of Biochemistry.

[⊥] Present address: Department of Biology, Center for Biotechnology and Interdisciplinary Studies, 1W14 Jonsson-Rowland Science Center, Rensselaer Polytechnic Institute, 110 Eighth Street, Troy, NY 12180-3590.

[1] Abbreviations: NOR, nitric oxide reductase; PDB, Protein Data Bank; SPDBV, Swiss PDB Viewer; DFT, density functional theory; cNOR, cytochrome *c* nitric oxide reductase; rmsd, root-mean-square deviation.

10.1021/bi050464f CCC: $30.25
Published on Web 07/21/2005

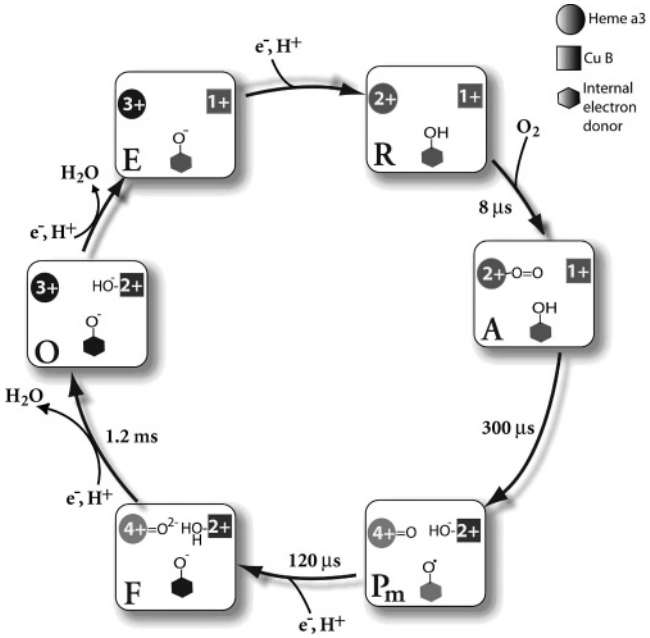

FIGURE 1: Catalytic cycle of cytochrome *c* oxidase, showing the role of the active-site tyrosine.

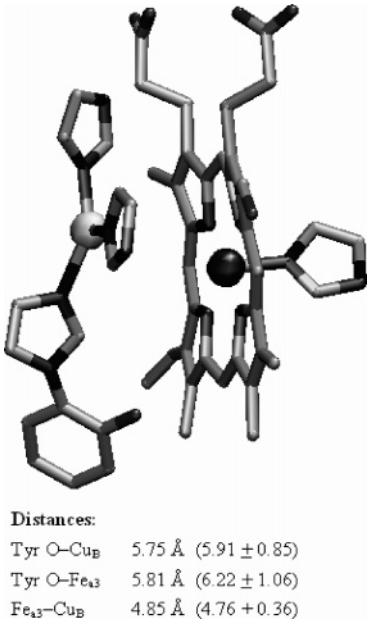

FIGURE 2: Active-site structure of *B. taurus* oxidase. The active site of *B. taurus* (2OCC) showing the cross-link between N_ϵ of the histidine imidizole (His240) and C_ϵ of the tyrosine phenol (Tyr244). The farnesyl tail of heme a_3 has been removed for clarity. The table gives the distances between the three redox active atoms: Cu_B, the heme Fe_{a3}, and the phenolic oxygen of the active-site tyrosine. The first number is the *B. taurus* distance, and the second number is the average distance of all known crystal structures.

heme−copper active site, where O_2 binds and is reduced to water. The binuclear center consists of a five-coordinate high-spin heme and a copper ion, Cu_B, ligated to three histidines. Six completely conserved histidine residues coordinate the low-spin heme, high-spin heme, and Cu_B, and the presence of these six histidines is diagnostic for members of the superfamily.

The active sites of the type A and B oxidases also contain a tyrosine residue that has been proposed to be important in the catalytic mechanism of the enzyme. This tyrosine (Tyr244, *Bos taurus*) is thought to donate a hydrogen atom (an electron plus a proton) during catalysis to facilitate cleavage of the O−O bond, resulting in the transient formation of a tyrosyl radical intermediate (A → P_m in Figure 1) (*23*−*28*). Attempts to replace this tyrosine in type A bacterial oxidases by site-directed mutagenesis have not succeeded to identify any substitution that will support oxidase activity. The physical location of this tyrosine and its total conservation in all of the type A and B oxidases strongly suggest that it plays a critical role in the catalytic mechanism.

One argument for the transient formation of a radical at this position is the fact that, in the X-ray structures of the *B. taurus* cytochome *aa*$_3$ (*15*), *P. denitrificans* cytochrome *aa*$_3$ (*18*, *19*), and *T. thermophilus* cytochrome *ba*$_3$ (*21*), this tyrosine is cross-linked to a nearby histidine (Tyr244−His240, *B. taurus*) which is one of the ligands to Cu_B. Possibly, the His-Tyr cross-link is formed as a side reaction of the putative tyrosyl radical during the initial turnovers of the enzyme. The cross-link (Figure 2), which has been confirmed chemically in the *T. thermophilus* cytochome *ba*$_3$ (*29*, *30*) joins the N_ϵ nitrogen of the histidine imidizole and the C_ϵ carbon of the tyrosine phenol (*15*, *19*, *21*). The fully oxidized, fully reduced, CO-bound, and azide-bound forms of bovine cytochrome *c* oxidase all have electron densities compatible with the His-Tyr cross-link, suggesting that it is present throughout the catalytic cycle (*15*). Whether the cross-link is critical to enzyme function is not known, but it does seem to have a role in maintaining the structure of the active site (*31*, *32*).

Sequence alignments show that all known type A and B oxidases, without exception, contain the active-site tyrosine. In contrast, sequence alignments (*6*) show this residue to be missing in all of the type C (*cbb*$_3$) oxidases, raising the important question of whether the type C oxidases might employ a different catalytic mechanism for facilitating the splitting of the O−O bond. The cytochrome *cbb*$_3$ oxidases have a glycine or alanine at the equivalent position in sequence alignments. Conceivably, the glycine but not alanine could act as a hydrogen atom donor, as observed in pyruvate:formate lyase (*33*), but neither glycine nor alanine could serve as a proton donor.

There is no crystal structure available for any type C oxidase (*34*); therefore, the structure of the active site cannot be examined to see what might replace the function of the active-site tyrosine. In this work, homology modeling, quantum chemistry, and molecular dynamics are used to predict the structure of subunit I (CcoN) of the *cbb*$_3$ oxidase from *V. cholerae*. The structural model predicts a tyrosine at the same spatial location at the enzyme active site but which comes from a different location in the sequence than the tyrosine observed in the type A and B oxidases. The active-site tyrosine in the *cbb*$_3$ oxidases is located in transmembrane helix VII, whereas the active-site tyrosine observed in the type A and B oxidases is located in transmembrane helix VI. Furthermore, the predicted active-site tyrosine in the type C oxidases is completely conserved within the family of *cbb*$_3$ oxidases. In the type A and B oxidases, the sequence position of the active-site tyrosine in the type C oxidases is occupied mostly by glycine and alanine residues.

Table 1: Template Proteins Used in Modeling

organism	PDB ID	hemes[a]	family	resolution (Å)	reference
P. denitrificans	1AR1	aa_3	A	2.7	*14, 15*
B. taurus	2OCC	aa_3	A	2.3	*11*−*13*
E. coli	1FFT	bo_3	A	3.5	*18*
T. thermophilus	1EHK	ba_3	B	2.4	*17*
R. sphaeroides	1M56	aa_3	A	3.5	*16*

[a] First and second letters refer to the low-spin and high-spin heme, respectively.

Site-directed mutagenesis experiments were performed to substitute for the predicted active-site tyrosine (Y255) in subunit I of the cbb_3 oxidase from *V. cholerae*. The Y255F mutant is assembled and has normal spectroscopic features but is completely inactive catalytically, consistent with a likely role of this tyrosine in catalysis. Establishing whether this tyrosine is post-translationally cross-linked to a histidine at the active site will require further work.

THEORETICAL METHODS

Sequence Mining and Alignment. Sequences homologous to known heme−copper oxidases were found using BLAST searches of the SDSC nonredundant protein database (*35*), the NCBI Microbial Genome Database (*36*), the TIGR Comprehensive Microbial Resource (*37*), the DOE JGI Microbial Database (*38*), and independent databases found within the GOLD Genomes Online Database (*39*). Over 500 prokaryotic members of the heme−copper oxidase superfamily were found, and a complete list is provided in the Supporting Information. All of the sequences were clustered into the known families: type A, B, and C oxidases and the nitric oxide reductases. Sequence alignments for each family were calculated separately using CLUSTAL W (*40*). Next, alignments between the individual families were performed to generate an alignment for the whole superfamily, which is needed to align the target sequence to the template structures. Secondary structural analyses were performed to ensure that the sequence alignments generated were consistent with predicted transmembrane helices. TMAP (*41*) was used to predict transmembrane regions from the multiple sequence alignments of the individual families.

Homology Modeling. Structural models for subunit I (CcoN) of the cbb_3 oxidase from *V. cholerae* were generated using homology modeling. Templates were found using a PSI-BLAST (*42*) search of the Protein Data Bank (PDB) (*43*) with the Biology Workbench interface (*35*). Proteins selected for use as templates in modeling are shown in Table 1. Homology models were generated using Swiss-Model via the Swiss PDB Viewer (SPDBV) interface (*44*, *45*). The low-spin heme, high-spin heme, and Cu_B ion were placed into the models using SPDBV by structurally aligning the model structures with the crystal structure of the *P. denitrificans* oxidase and overlaying the cofactors. The A-type hemes in the *P. denitrificans* oxidase were then converted to B-type hemes, which are present in the cbb_3 oxidases. Water molecules were added to the models using DOWSER (*46*). All water molecules placed by DOWSER with stabilization energies greater than 12 kcal/mol were included in the models.

Simulated Annealing. Structural refinement of the models was carried out with a simulated annealing procedure using NAMD2 (*47*) and the CHARMM27 proteins and lipids release force field (*48*), modified as described below. The hemes and copper were allowed to relax via the steepest descent minimization, keeping the α-carbon atoms fixed. All constraints were removed, and the system was heated to 400 K using Langevin dynamics for 250 ps. The temperature was then reduced by 10%, and dynamics was performed for another 250 ps. This procedure was iterated until the temperature dropped below 290 K, at which point the system was quenched to its nearest local minimum using conjugate-gradient minimization. The total simulation time for each model was 1 ns.

Force-Field Modifications. We refined structures for active sites in different redox states either with or without a His-Tyr cross-link. The fully oxidized state was modeled using hydroxide as a metal ligand for both the high-spin heme and Cu_B, while the one-electron reduced state was modeled using hydroxide as the metal ligand for the high-spin heme. Atomic charges for the active site in different redox states are determined from Mulliken analysis (*49*) of the electronic wave function obtained by quantum mechanical modeling. Hybrid density functional theory, DFT-B3LYP (*50*), and the LA3VP effective core potential (*51*) and basis set (*52*) were used on a model binuclear center prepared as described previously (*14*). Bond and angle equilibrium values for the copper ligands were taken from an average of the published X-ray crystal structures. The force constants used were set to 65 kcal/mol Å^2 for bonds and 30 kcal/rad^2 for the angles (*13*). Where the His-Tyr cross-link was included, the equilibrium $N_\epsilon-C_\epsilon$ bond distance was taken to be the average value (1.4 Å) from published structures with known His-Tyr cross-links (*15*−*22*). A bond force constant of 400 kcal/mol Å^2 was used.

EXPERIMENTAL PROCEDURES

Mutagenesis of cbb_3 Oxidase. Site-directed mutagenesis was performed using Stratagene QuikChange kits. The oligonucleotides used for mutagenesis, Y255F-F 5′-GGCTCTGATTTCTCTCTTTATTTGGGCAGGTCCGC-3′ and Y255F-R 5′-GCGGACCTGCCCAAATAAAGAGAGAAATCAGAGCC-3′, were synthesized by Qiagen. The restriction enzymes were from New England Biolabs and Gibco-BRL. Mutagenesis was verified by sequencing performed at the Biotechnology Center at the University of Illinois Urbana-Champaign.

Purification of Overexpressed Proteins. V. cholerae cells containing plasmids for the desired polyhistidine-tagged protein were grown in LB media (USB Corporation) with 100 μg/L ampicillin (Fisher Biotech) and 100 μg/L streptomycin (Sigma) at 37 °C. Cells were grown to 60 Klett units, and then gene expression was induced with 0.2% L-(+)-arabinose (Sigma). At 150 Klett units, the cells were collected by centrifuging at 7000 rpm for 30 min. The cells were then frozen overnight at −80 °C. Thawed cells were homogenized on ice with DNAase I (Sigma) and PMSF. Cells were then lysed by five passes through a disruptor and centrifuged at 40000 rpm overnight to collect membranes. Membrane proteins were solubilized by adding 0.5% dodecyl β-D-maltoside (Anatrace) and shaken at 4 °C for 30 min. Nonsolubilized membranes were removed by centrifuging at 40000 rpm for 30 min. The enzyme was purified using Ni^{2+}-NTA agarose resin obtained from Qiagen.

Heme Analysis of Proteins. Proteins were separated on GeneMate Express PAGE Gels from ISC BioExpress. Gels were then soaked in 3 parts 6.3 mM 3,3′,5,5′-tetramethylbenzidine (TMBZ from Sigma) and 7 parts 0.25 M sodium acetate at pH 5.0 for 1 h. Gels were stained for heme by adding H_2O_2 to 30 mM. This procedure revealed the subunits containing covalent heme c.

Ratios of heme c/heme b were calculated from the reduced-minus-oxidized difference spectra using Matlab. For heme c, the wavelength pair 550/540 nm was used with an extinction coefficient of 20 mM^{-1} cm^{-1}. For heme b, 560/580 nm with an extinction coefficient of 25 mM^{-1} cm^{-1} was used.

Spectroscopic Analysis. Spectra were acquired using an Agilent Technologies 8453 UV−vis spectrophotometer with ChemStation software. A total of 25 μL of the protein sample was mixed with 100 μL of 50 mM sodium phosphate buffer, 0.05% DM, and 5% glycerol at pH 8.0. The enzymes were oxidized with 2 μL of 1 mM $FeCN_6$ and reduced with dithionite, both obtained from Sigma. Spectra were measured from 375 to 850 nm and analyzed using Matlab.

Oxidase Activity Measurements. A YSI model 53 oxygen monitor was used to polarographically measure steady-state oxidase activity. The buffer used for oxidase activity measurements was 50 mM sodium phosphate and 50 mM NaCl at pH 8.0. A total of 10 μL of 1 M ascorbate and 18 μL of 0.1 M TMPD were mixed with 1.8 mL of buffer in the sample chamber at 25 °C. The reaction was initiated by adding 10 μL of 1 μM enzyme, and oxygen consumption was monitored.

RESULTS

Structural Modeling. As detailed in the Theoretical Methods, all currently sequenced heme−copper oxidases from annotated databases and genome-sequencing projects were used to generate a multiple sequence alignment. Over 500 prokaryotic members of the heme−copper oxidase superfamily were found (a complete listing is given in the Supporting Information.) All of the sequences were clustered into the known families: type A oxidases, type B oxidases, type C oxidases, and the nitric oxide reductases. The type C oxidases consisted of a total of 120 *cbb*$_3$ oxidase homologues. Sequence alignments for each of the heme−copper oxidase families were calculated separately. Sequences within each family are similar, and within-family alignments are easily calculated. Next, alignments between the individual families were performed to generate an alignment for the whole superfamily. Secondary structural analyses were performed to ensure that the sequence alignments generated were consistent with predicted transmembrane helices. To assess the expected accuracy of this procedure, it was also applied to oxidases of known crystal structure. The results are shown in Figure 3. The transmembrane helix prediction worked well for members of both type A and B families. This figure also shows the predicted location of the transmembrane helices in the *V. cholerae cbb*$_3$ oxidase, for which there is no crystal structure. It should be noted that, in the region surrounding the active site, the sequence alignment is anchored by absolutely conserved metal-ligating histidine residues. Thus, it is highly unlikely that the sequences are misaligned within the core of the protein.

Sequence alignments of the *cbb*$_3$ oxidase family to the template families showed significant sequence homology in all helices with the exception of helices IV and V. In both of these helices, however, the predicted transmembrane regions from the *cbb*$_3$ oxidase family aligned well with the transmembrane regions of the template families. To improve alignments in theses helices, the *cbb*$_3$ oxidase family was aligned to the cytochrome *c* nitric oxide reducatse (cNOR) family, which is also part of the superfamily that is paralogous with the oxidases and have been proposed to be structurally similar to the oxidases (*53*). Alignments between the *cbb*$_3$ oxidase and the cNOR families show that the cNORs have very short interhelical turns, which makes them useful in defining the helical boundaries. When the alignments between the *cbb*$_3$ oxidase family and the cNOR family are compared to the predicted transmembrane helices, alignments for helices IV and V were generated. The alignment for these two helices generated in this way agrees well with the alignment between the *cbb*$_3$ oxidase family and the template families generated by profile alignment, adding confidence to the alignment of the whole superfamily. The target−template alignment used in homology modeling was extracted from the complete superfamily alignment, shown in Figure 3.

The percent sequence identity and the α-carbon root-mean-square deviation (rmsd) for each pair of templates used in modeling are shown in Table 2. Because each protein varies in the number of residues located in each interhelical loop, it is not possible to obtain rmsd values for the whole protein. Instead, we report rmsd values for the core of the protein and the maximum structural overlap. The core of the protein is defined to be all 12 transmembrane helices and contains all of the residues necessary for the formation of both the active site and the proton channels. The maximum structural overlap is defined to be all of the residues in the core and those loop regions that overlap structurally. As expected, pairs of templates with high sequence identity are also structurally very similar. There are four pairs of templates with sequence identities less than 20%; however, their average α-carbon rmsd is only 1.87 Å for the core region and 2.21 Å for the maximum structural overlap. Even templates with low sequence identity are similar structurally, highlighting the high degree of structural conservation of the heme−copper superfamily.

The structures resulting from homology modeling were refined in different redox states with and without an active-site His-Tyr cross-link, using ligands appropriate for each redox state as described in the Experimental Procedures. As a further test, the same procedure was applied to generate structural models for oxidases of known crystal structure, using only the information from other crystal structures in homology modeling. Table 3 shows the results of all of these control models. The model for *T. thermophilus*, which is a member of the type B family, has a rmsd of 1.89 Å using only type A oxidases as templates. It is seen that our procedure generates accurate models for the heme−copper oxidase superfamily even when the sequence to be modeled is not a member of families to which the templates belong.

Homology modeling is usually only performed if the sequence of interest has at least 25% sequence identity to the structures used in the modeling. This is because the structures tend to rapidly diverge at low sequence identities.

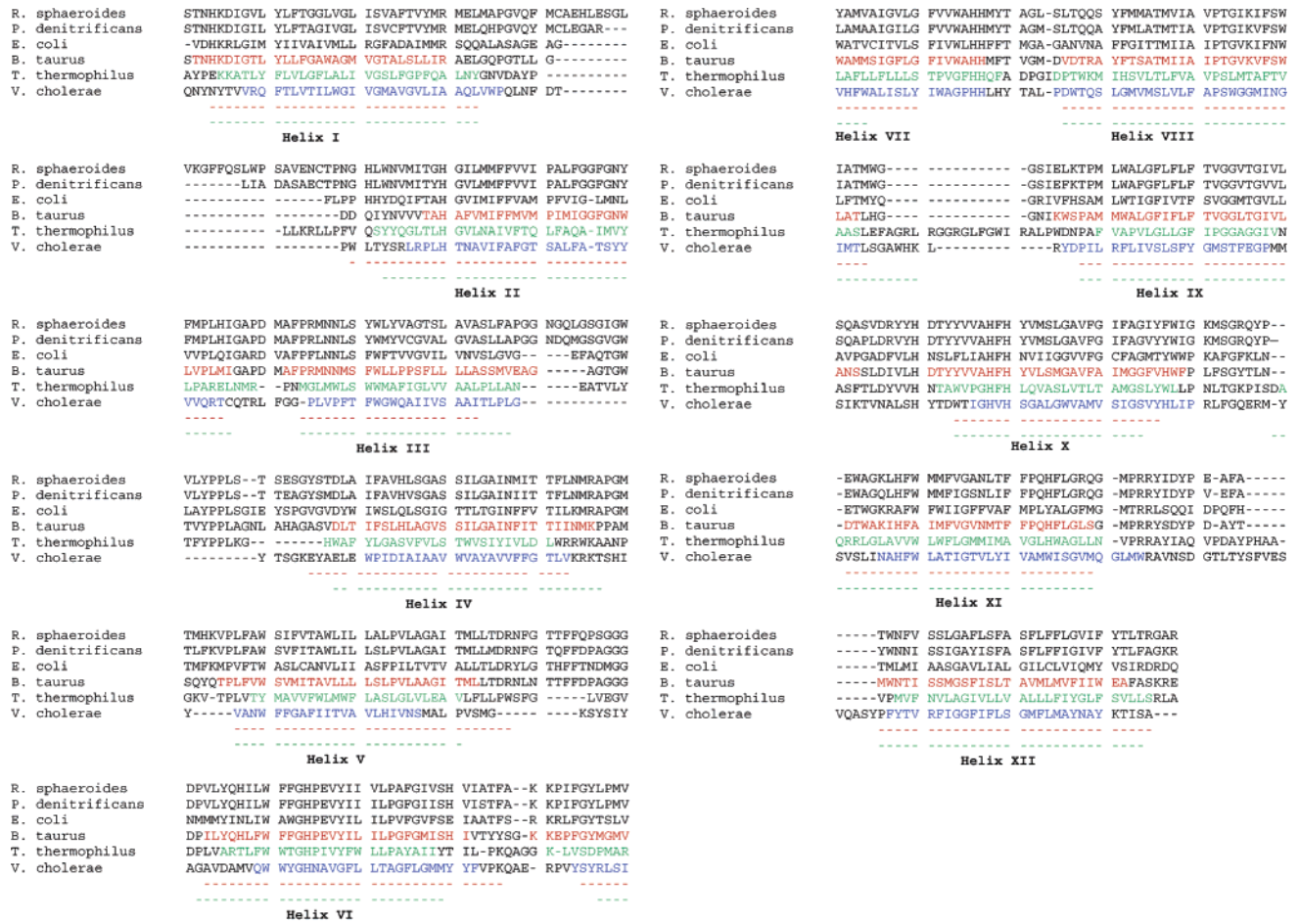

FIGURE 3: Sequence alignment and transmembrane helix prediction results. The transmembrane regions for all of the heme−copper oxidase families were predicted from multiple sequence alignments using TMAP. Below is the sequence alignment of *V. cholerae* versus the template proteins used in modeling (listed in Table 1). TMAP predictions for a member of each family are shown. The predicted transmembrane regions are colored according to the family type, while the approximate transmembrane helices determined from the crystal structure are shown in dashes below the alignment. The type A family is represented by *B. taurus* (red), the type B family by *T. thermophilus* (green), and the type C family by *V. cholerae* (blue).

Table 2: Pairwise Comparison of All Template Proteins (B = *B. Taurus*, P = *P. denitirificans*, R = *R. sphaeroides*, E = *E. coli*, T = *T. thermophilus*) Used in the Modeling Process[a]

templates	% sequence identity	α-carbon rmsd (Å) (core/maximum overlap)
P−R	81	0.96/0.42
B−P	53	1.07/0.65
B−R	52	0.59/0.62
E−B	38	1.02/1.07
E−P	36	1.36/1.08
E−R	34	0.97/1.01
T−P	18	1.93/2.15
T−B	18	1.87/2.26
T−R	17	1.77/2.16
T−E	13	1.90/2.28

[a] The first column is the pair of proteins compared; the second column is the percent sequence identity between the pair of proteins; and the third column is the calculated rmsd as described in the text. Even protein pairs with a low sequence identity have very similar structures.

However, the results in Table 2 show that, for the heme−copper oxidases, as little as 13% sequence identity results in significant structural overlap. The heme−copper oxidases constitute a remarkably structurally conserved protein family. Hence, homology modeling can be successful even when the sequence identity is low. This is shown explicitly in Table 3. The *T. thermophilus* cytochrome ba_3 has an average sequence identity of only 16% with the templates used in the control models, but homology modeling predicts an acceptable structure. This gives us confidence in the modeling procedure for cbb_3 oxidases.

Table 3: Control Models Were Generated for Each Template Protein as Described in the Text[a]

model (family)	core α-carbon rmsd	templates
P. denitirificans (A)	0.47	B, E, R, T
B. taurus (A)	0.61	E, P, R, T
E. coli (A)	0.95	B, P, R, T
R. sphaeroides (A)	0.40	B, E, P, T
T. thermophilus (B)	1.89	B, E, P, R

[a] The rmsd values between the models and the crystal structure are shown in the table. Templates used in generating the control model structure are shown using the abbreviations listed in Table 2. Note that all templates used to construct the *T. thermophilus* model (a type B oxidase) are type A oxidases.

Active-Site Tyrosine. The models generated for *V. cholerae* cbb_3 oxidase show the presence of an active-site tyrosine analogous to Tyr244 from the *B. taurus* oxidase. The tyrosine (Tyr255, *V. cholerae* numbering) is located in transmembrane helix VII and occupies the same spatial position in the protein as does the bovine active-site tyrosine (Figure 4a). Sequence alignments show that this tyrosine is absolutely conserved

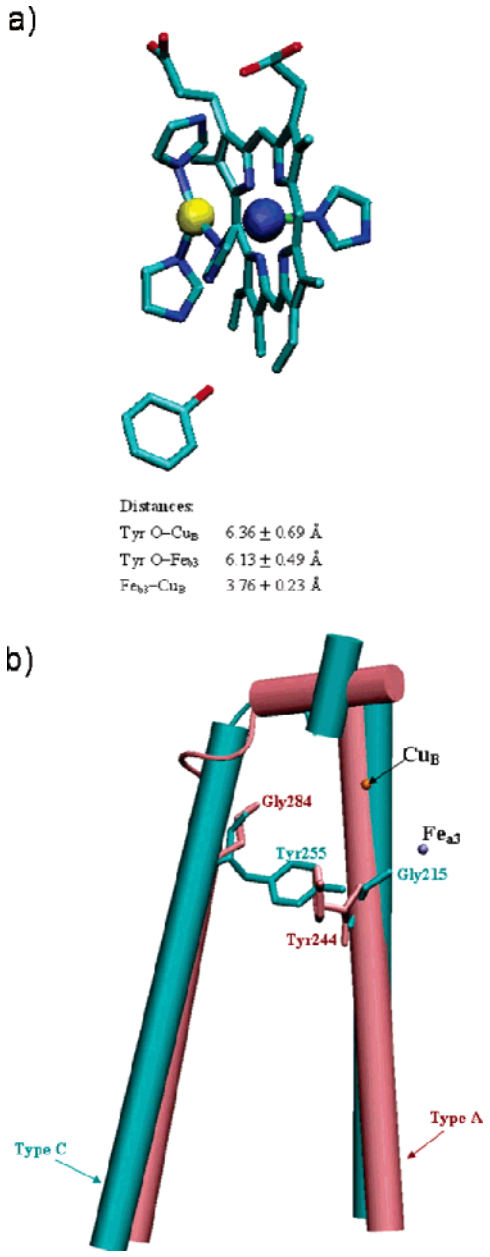

FIGURE 4: Predicted active-site structure of *V. cholerae*. The structures shown are from models of the fully oxidized state with no cross-link enforced. (a) Active-site model of *V. cholerae* cbb_3 oxidase. The table gives the distances between the three redox active atoms: Cu_B, the heme Fe, and the phenolic oxygen of the active-site tyrosine. The distances are the average of all replicates of the simulations. (b) Cartoon of the active-site tyrosine demonstrating the helix switching between helix VI and VII. *B. taurus* is shown in pink, and *V. cholerae* is shown in cyan.

among the cbb_3 oxidases. This is an unexpected structural feature that is unique to the cbb_3 oxidases.

Figure 5 shows the sequence alignment of helices VI and VII of the cbb_3 oxidase from *V. cholerae* with the oxidases whose crystal structures are known, indicating the sequence position of the active-site tyrosine. In type A and B oxidases, the sequence position that is occupied by the proposed active-site tyrosine in the cbb_3 oxidases is always a small residue (glycine, alanine, or serine). In the cbb_3 oxidases, the sequence position occupied by the active-site tyrosine in the type A and B families is also always a small residue (glycine or alanine). Apparently, during the evolution of the heme–copper oxidases, the active-site tyrosine migrated from one helix to another with the concomitant exchange of a small residue to conserve the active-site volume. This is an example of "residue hopping," where residues that have the same catalytic role are not located in the same position in the structure-based sequence alignment (*54*–*56*). Figure 4b compares the two helices in the *B. taurus* and *V. cholerae* structures, highlighting this "residue hopping". It is currently not known how the observed structural change would affect enzymatic properties such as oxygen affinity and catalytic rate.

		Helix VI
Type A	*R. sphaeroides*	VLYQHILWFFGHPEVYIIVLPAFGIVS
	P. denitrificans	VLYQHILWFFGHPEVYIIILPGFGIIS
	B. taurus	ILYQHLFWFFGHPEVYILILPGFGMIS
	E. coli	MMYINLIWAWGHPEVYILILPVFGVFS
Type B	*T. thermophilus*	LVARTLFWWTGHPIVYFWLLPAYAIIY
Type C	*V. cholerae*	AVDAMVQWWYGHNAVGFLLTAGFLGMM

		Helix VII
Type A	*R. sphaeroides*	GYLPMVYAMVAIGVLGFVVWAHHMYT
	P. denitrificans	GYLPMVLAMAAIGILGFVVWAHHMYT
	B. Taurus	GYMGMVWAMMSIGFLGFIVWAHHMFT
	E. coli	GYTSLVWATVCITVLSFIVWLHHFFT
Type B	*T. thermophilus*	SDPMARLAFLLFLLLSTPVGFHHQFA
Type C	*V. cholerae*	SYRLSIVHFWALISLYIWAGPHHLHY

FIGURE 5: Helix switching of the active-site tyrosine. The sequence location of the active-site tyrosine has switched between helix VI and VII. Residues conserved in all heme–copper oxidases are shown in blue. The conserved active-site tyrosine from type A and B heme–copper oxidases is located in helix VI, while the predicted active-site tyrosine from the type C heme–copper oxidases is found in helix VII. The active-site tyrosine is shown in red.

Table 4: Comparison of Different Type C Oxidase Models (V = *V. cholerae*, R = *R. sphaeroides*, S = *S. azorense*) Generated Using the Procedures Detailed in the Text

models	% sequence identity	core α-carbon rmsd (Å)
V–R	62	1.51
V–S	29	1.59
R–S	26	1.55

To explore the generality of this residue hopping, we have carried out the same homology modeling and structure refinement procedure for two other type C oxidases from *Sulfurihydrogenibium azorense* and *R. sphaeroides*. Note that the *R. sphaeroides* genome has both type A and C oxidases, and these should not be confused. The sequence similarity and resulting rmsd among the three type C oxidases that we have modeled are presented in Table 4. In Figure 6, we show a superposition of the structural models, highlighting the active-site tyrosine, which has migrated to a different helix compared to type A and B oxidases.

To determine whether a cross-link between Tyr255 and His262 (*V. cholerae* cbb_3 oxidase) is possible in the cbb_3 oxidases, the protein was simulated in four different states of the active site. In the simulations, the active site had a net charge of +2 and +1, to mimic the fully oxidized (O) and one-electron reduced (E) states, respectively. A cross-link was also imposed between the C_ϵ of Tyr255 and the N_ϵ of His262 in both the fully oxidized and one-electron reduced states. The resulting structures were refined as described in the Experimental Procedures. The active-site region was compared to known heme–copper oxidase structures as shown in Table 5 (residues used in defining the active site

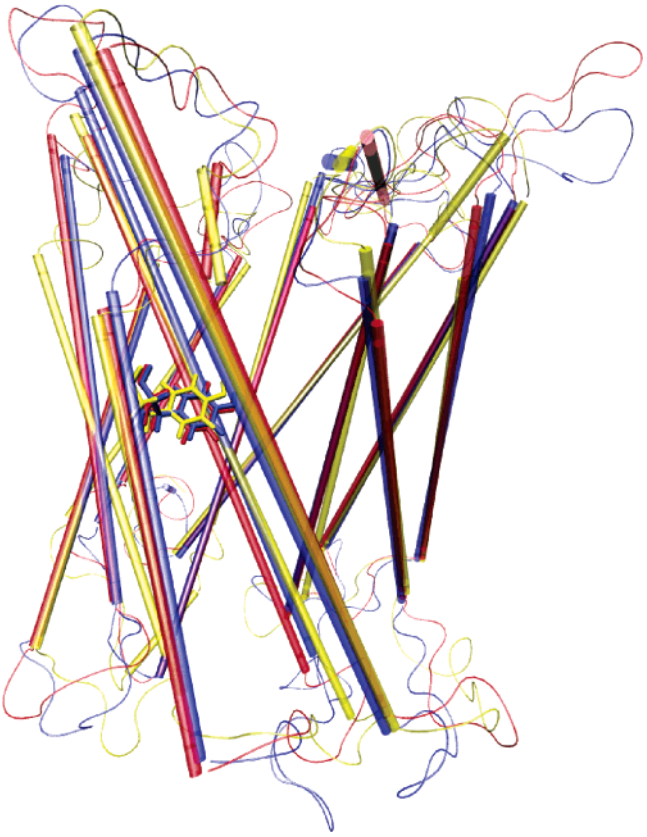

FIGURE 6: Comparison of structure prediction results for three different type C oxidases: *V. cholerae* (blue), *S. azorense* (yellow), and *R. sphaeroides* (red). The active-site tyrosine is shown in each case. The close agreement concerning the position of the active-site tyrosine supports the generality of the results presented here.

Table 5: Active-Site Comparisons[a]

	conserved active-site rmsd (Å)		
	histidines only	all side chains	TyrOH distance
B. taurus	0.00/1.29	0.00/1.30	0.00
R. sphaeroides	0.00/1.29	0.46/1.43	0.13
P. denitirifcans	0.43/1.32	0.72/1.55	0.83
E. coli	0.50/1.40	1.84/1.86	2.57
T. thermophilus	0.48/1.32	0.61/1.30	0.55
V. cholerae (E)	2.95/1.79	2.87/1.66	1.84
V. cholerae (O)	2.95/1.73	3.60/2.48	0.91
V. cholerae (E) cross	2.92/1.71	2.53/1.47	2.36
V. cholerae (O) cross	2.97/1.74	2.69/1.75	1.94
average	1.53	1.64	1.39

[a] In the first two columns, the first number is the rmsd compared to the *B. taurus* active site, while the second number is the rmsd compared to the average structure of all of the active sites listed. The third column is a measure of the distance between the tyrosine O of the *B. taurus* active site and the tyrosine O of the listed active site. The residues used in the comparison are listed in Table 6.

are listed in Table 6). Agreement with known structures is best when the cross-link is enforced, but the results cannot unambiguously resolve the question as to whether this cross-link is present in *V. cholerae*. Distances between the tyrosine oxygen atom and the active-site metal ions are given in Table 7, compared to the same distances in oxidases with known crystal structures.

In the fully oxidized state, the tyrosine was found to be at the same location regardless of whether the cross-link was enforced (Figure 7). This implies that the tyrosine is in the correct location for a cross-link to be easily formed. The cross-link in the type A and B oxidases is formed between residues on the same helix (VI) separated by one helical turn. In the *cbb*$_3$ oxidases, an interhelical cross-link would be formed between helices VI and VII. This interhelical cross-link could modify the dynamics of the protein because two of its helices would be coupled together. In particular, it might be expected to lead to increased structural rigidity.

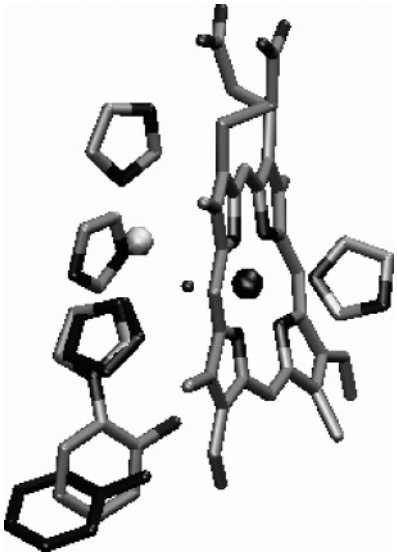

FIGURE 7: *V. cholerae cbb*$_3$ oxidase fully oxidized (O) active site with and without the modeled cross-link. The active-site tyrosine and histidine from simulations without a cross-link are shown in black. The distance from N_ϵ nitrogen of the histidine imidizole to the C_ϵ carbon of the tyrosine phenol is 3.30 Å without the cross-link and 1.12 Å with the cross-link enforced.

In the one-electron reduced state with a cross-link enforced, the tyrosine was in the same conformation as it was in the oxidized state. However, in the one-electron reduced state without the cross-link, the tyrosine was facing down toward the cytoplasmic side of the protein in half of the simulations. This suggests that either the cross-link is necessary for the correct formation of the active site, or if the cross-link is not necessary, the tyrosine may be involved in a proton-shuttling mechanism. Simulations of the one-electron reduced state without the cross-link show that the active-site tyrosine forms a hydrogen-bonding network with a water molecule and a completely conserved tyrosine (Tyr321) that is located in the putative proton-conducting "K-channel" (*57*) for the *cbb*$_3$ oxidases (Figure 8). In the absence of a cross-link, this could act as a gate for proton delivery to the active site after reduction. Chemical verification of the cross-link is necessary to determine which of these mechanisms are functioning in the *cbb*$_3$ oxidases.

Mutagenesis. To verify the predictions made from modeling, site-directed mutagenesis studies were performed on the *cbb*$_3$ oxidase from *V. cholerae*. The active-site tyrosine was mutated to phenylalanine (Y255F), and its properties were compared to the wild-type (wt) enzyme. The Y255F mutant had been assembled correctly as evidenced by heme staining, heme composition, and optical spectroscopy. A heme-staining gel of the Y255F and wt enzymes (Figure 9) shows identical staining for both of the heme c containing subunits of the *cbb*$_3$ oxidase complex. Including the hemes, CcoP has a predicted mass of 37.1 kD and CcoO has a predicted mass of 24.2 kD. Heme staining identifies two bands, one at ~37

Table 6: Conserved Residues in Heme−Copper Oxidase Active Site[a]

R. sphaeroides	*P. denitrificans*	*E. coli*	*T. thermophilus*	*B. taurus*	*V. cholerae*
His284	His276	His284	His233	His240	His211
His333	His325	His333	His282	His290	His261
His334	His326	His334	His283	His291	His262
His419	His411	His419	His384	His376	His349
Tyr288	Tyr280	Tyr288	Tyr237	Tyr244	Tyr255
Val287	Val279	Val287	Val236	Val243	Val214
heme a_3	heme a_3	heme o_3	heme a_3	heme a_3	heme b_3
Cu_B	Cu_B	Cu_B	Cu_B	Cu_B	Cu_B

[a] Listed are the residues used in the active-site comparisons along with their respective numbering.

Table 7: Comparison of the Distances (in Angstroms) from the Active-Site Tyrosine Oxygen to the Active-Site Metals[a]

	TyrOH (active-site Cu)	TyrOH (high-spin Fe)
B. taurus	5.75	5.81
R. sphaeroides	5.78	5.82
P. denitrificans	5.02	5.52
E. coli	7.32	8.43
T. thermophilus	5.51	5.82
average	5.88 ± 0.86	6.28 ± 1.20
V. cholerae (O)	5.44 ± 0.51	5.79 ± 0.34
V. cholerae (E)	5.46 ± 0.51	5.44 ± 0.84

[a] Values given for *V. cholera* are for models with the cross-link enforced.

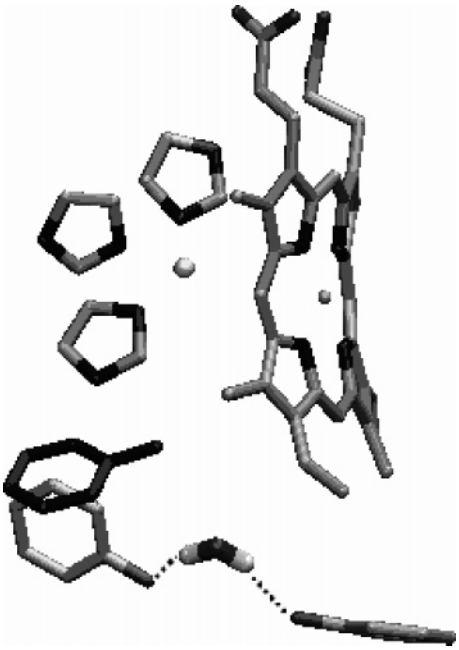

FIGURE 8: Potential K-channel proton gate. In simulations of the *V. cholerae* one-electron reduced state without a His-Tyr cross-link, the active-site tyrosine is sometimes found facing away from the active site, forming a hydrogen-bond network with a water molecule and a completely conserved tyrosine (Y321) residue. This could potentially act as a redox-state-dependent proton gate. The active-site tyrosine in the oxidized state is shown in black, while the same residue in the one-electron reduced state is shown in gray.

kD and the other at ~24.5 kD. Heme c/heme b ratios were calculated from reduced minus oxidized spectra. A value of 2.19 was obtained for the wt and 2.18 for the Y255F enzyme.

Optical spectra of the reduced minus oxidized state and the fully reduced state for both enzymes are shown in Figure 10. The fully reduced spectra are virtually identical (Figure 10b), while the reduced minus oxidized spectra show only minor differences (Figure 10a). This demonstrates that the active site of the Y255F mutant is correctly assembled with minimal structural perturbation.

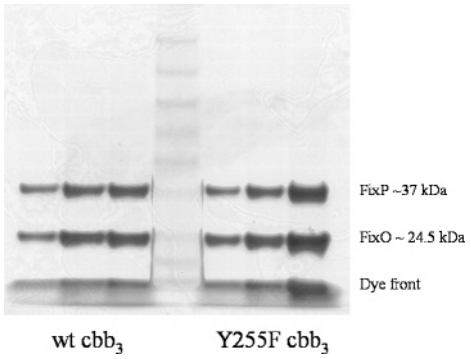

FIGURE 9: Heme staining of wild type (wt) and mutant (Y255F) *cbb*$_3$ oxidase. TMBZ was used to stain for the presence of hemes. Both CcoO and CcoP contain covalently attached heme c. CcoP has a predicted mass of 37.1 kDa and migrates at ~37 kDa, while CcoO has a predicted mass of 24.2 kDa and migrates at ~24.5 kDa. The heme staining at the dye front is probably due to the noncovalently attached heme b from CcoN. Lanes 1−3 contain 1, 2.5, and 5 μL of wt *cbb*$_3$, Lane 4 is the BenchMark prestained protein ladder. Lanes 5−7 contain 1, 2.5, and 5 μL of Y255F *cbb*$_3$.

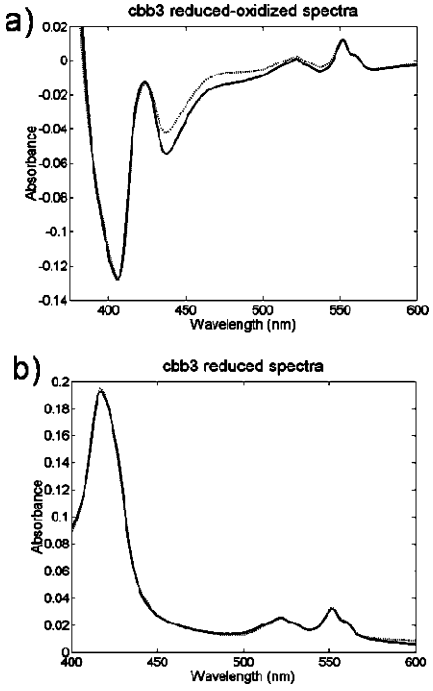

FIGURE 10: UV−vis spectra of wild type (wt) and mutant (Y255F) *cbb*$_3$ oxidase. The reduced minus oxidized (a) and the reduced spectra (b) are shown for both wt and Y255F. The wt is the solid line, and the Y255F mutant is the dashed line. The mutation caused virtually no difference in the spectra, which implies that the active-site structure is minimally perturbed by the mutation.

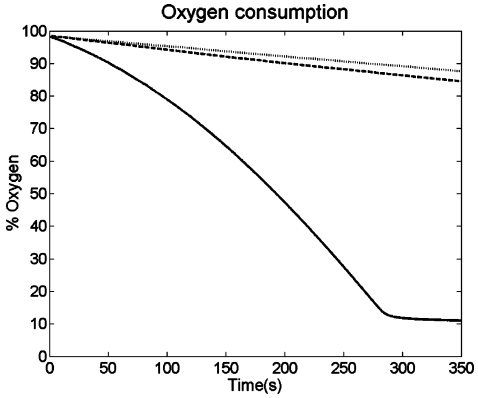

FIGURE 11: Oxygen consumption measurements. The solid line is the oxygen consumption measured for the wild-type cbb_3 oxidase as described in the text. The dotted line is the oxygen consumption of the Y255F mutant. The dashed line is the control sample with no oxidase added. The Y255F mutant has no catalytic activity.

To test the activity of the Y255F and wt enzymes, oxygen consumption rates were measured. Figure 11 shows the oxygen consumption of both enzymes. The Y255F mutant is completely inactive. This verifies the prediction that the active-site tyrosine plays a role in the catalytic cycle of the type C oxidases.

CONCLUSIONS

The present work reports the first structural models of a cbb_3 (type C) oxidase. These models predict the presence of a previously unknown active-site tyrosine, with the possibility of a His-Tyr cross-link post-translational modification analogous to those found in the type A and B oxidases. Mutagenesis studies show that the active-site tyrosine is crucial for catalytic activity in the type C oxidases. This work suggests that all heme−copper oxidases utilize the same catalytic mechanism for the reduction of O_2 to water. However, there remains the possibility of differences in the proton-pumping pathways, and we identified a possible shuttling mechanism involving the active-site tyrosine in *V. cholerae* cbb_3 oxidase. This shuttling mechanism is only feasible if the His-Tyr cross-link is not present. These results provide considerable impetus to determine if the His-Tyr cross-link is present in type C oxidases, and such work is currently in progress.

ACKNOWLEDGMENT

We thank Ashtamurthy Pawate for assistance in making Figure 1. Figures 2, 4, 6, 7, and 8 have been made with the VMD program (*58*).

SUPPORTING INFORMATION AVAILABLE

Complete list of all sequences used in analysis, along with their origin. This material is available free of charge via the Internet at http://pubs.acs.org.

REFERENCES

1. Malatesta, F., Antonini, G., Sarti, P., and Brunori, M. (1995) Structure and function of a molecular machine—Cytochrome *c* oxidase, *Biophys. Chem. 54*, 1−33.
2. Ferguson-Miller, S., and Babcock, G. (1996) Heme/copper terminal oxidases, *Chem. Rev. 96*, 2889−2908.
3. Schultz, B., and Chan, S. (2001) Structures and proton-pumping strategies of mitochondrial respiratory enzymes, *Annu. Rev. Biophys. Biomol. Struct. 30*, 23−65.
4. Garcia-Horsman, J., Barquera, B., Rumbley, J., Ma, J., and Gennis, R. (1994) The superfamily of heme−copper respiratory oxidases, *J. Bacteriol. 176*, 5587−5600.
5. Calhoun, M., Thomas, J., and Gennis, R. (1994) The cytochrome oxidase superfamily of redox-driven proton pumps, *Trends Biochem. Sci. 19*, 325−330.
6. Pereira, M., Santana, M., and Teixeira, M. (2001) A novel scenario for the evolution of haem−copper oxygen reductases, *Biochim. Biophys. Acta 1505*, 185−208.
7. Preisig, O., Anthamatten, D., and Hennecke, H. (1993) Genes for a microaerobically induced oxidase complex in *Bradyrhizobium japonicum* are essential for a nitrogen-fixing endosymbiosis, *Proc. Natl. Acad. Sci. U.S.A. 90*, 3309−3313.
8. Saraste, M., Castresana, J., Higgins, D., Lubben, M., and Wilmanns, M. (1997) in *Origin and Evolution of Biological Energy Conversion*, pp 255−289.
9. Vanderoost, J., Deboer, A., Degier, J., Zumft, W., Stouthamer, A., and Vanspanning, R. (1994) The heme−copper oxidase family consists of three distinct types of terminal oxidases and is related to nitric oxide reductase, *FEMS Microbiol. Lett. 121*, 1−9.
10. Blomberg, M., Siegbahn, P., Babcock, G., and Wikstrom, M. (2000) Modeling cytochrome oxidase: A quantum chemical study of the O−O bond cleavage mechanism, *J. Am. Chem. Soc. 122*, 12848−12858.
11. Medvedev, D., Daizadeh, I., and Stuchebrukhov, A. (2000) Electron-transfer tunneling pathways in bovine heart cytochrome *c* oxidase, *J. Am. Chem. Soc. 122*, 6571−6582.
12. Zheng, X., Medvedev, D., Swanson, J., and Stuchebrukhov, A. (2003) Computer simulation of water in cytochrome *c* oxidase, *Biochim. Biophys. Acta 1557*, 99−107.
13. Hofacker, I., and Schulten, K. (1998) Oxygen and proton pathways in cytochrome *c* oxidase, *Proteins 30*, 100−107.
14. Moore, D., and Martinez, T. (2000) *Ab initio* study of coupled electron transfer/proton transfer in cytochrome *c* oxidase, *J. Phys. Chem. A 104*, 2367−2374.
15. Yoshikawa, S., Shinzawaitoh, K., Nakashima, R., Yaono, R., Yamashita, E., Inoue, N., Yao, M., Fei, M., Libeu, C., Mizushima, T., Yamaguchi, H., Tomizaki, T., and Tsukihara, T. (1998) Redox-coupled crystal structural changes in bovine heart cytochrome *c* oxidase, *Science 280*, 1723−1729.
16. Tsukihara, T., Aoyama, H., Yamashita, E., Tomizaki, T., Yamaguchi, H., Shinzawa-Itoh, K., Nakashima, R., Yaono, R., and Yoshikawa, S. (1995) Structures of metal sites of oxidized bovine heart cytochrome *c* oxidase at 2.8 Å, *Science 269*, 1069−1074.
17. Tsukihara, T., Aoyama, H., Yamashita, E., Tomizaki, T., Yamaguchi, H., Shinzawaitoh, K., Nakashima, R., Yaono, R., and Yoshikawa, S. (1996) The whole structure of the 13-subunit oxidized cytochrome *c* oxidase at 2.8 Å, *Science 272*, 1136−1144.
18. Iwata, S., Ostermeier, C., Ludwig, B., and Michel, H. (1995) Structure at 2.8 Å resolution of cytochrome *c* oxidase from *Paracoccus denitrificans*, *Nature 376*, 660−669.
19. Ostermeier, C., Harrenga, A., Ermler, U., and Michel, H. (1997) Structure at 2.7 Å resolution of the *Paracoccus denitrificans* two-subunit cytochrome *c* oxidase complexed with an antibody F−V fragment, *Proc. Natl. Acad. Sci. U.S.A. 94*, 10547−10553.
20. Svensson-Ek, M., Abramson, J., Larsson, G., Tornroth, S., Brzezinski, P., and Iwata, S. (2002) The X-ray crystal structures of wild-type and EQ(I-286) mutant cytochrome *c* oxidases from *Rhodobacter sphaeroides*, *J. Mol. Biol. 321*, 329−339.
21. Soulimane, T., Buse, G., Bourenkov, G., Bartunik, H., Huber, R., and Than, M. (2000) Structure and mechanism of the aberrant ba_3-cytochrome *c* oxidase from *Thermus thermophilus*, *EMBO J. 19*, 1766−1776.
22. Abramson, J., Riistama, S., Larsson, G., Jasaitis, A., Svensson-Ek, M., Laakkonen, L., Puustinen, A., Iwata, S., and Wikstrom, M. (2000) The structure of the ubiquinol oxidase from *Escherichia coli* and its ubiquinone binding site, *Nat. Struct. Biol. 7*, 910−917.
23. Gennis, R. (1998) Multiple proton-conducting pathways in cytochrome *c* oxidase and a proposed role for the active-site tyrosine, *Biochim. Biophys. Acta 1365*, 241−248.
24. MacMillan, F., Kannt, A., Behr, J., Prisner, T., and Michel, H. (1999) Direct evidence for a tyrosine radical in the reaction of cytochrome *c* oxidase with hydrogen peroxide, *Biochemistry 38*, 9179−9184.

25. Proshlyakov, D., Pressler, M., DeMaso, C., Leykam, J., DeWitt, D., and Babcock, G. (2000) Oxygen activation and reduction in respiration: Involvement of redox-active tyrosine 244, *Science 290*, 1588−1591.
26. Tomson, F., Bailey, J., Gennis, R., Unkefer, C., Li, Z., Silks, L., Martinez, R., Donohoe, R., Dyer, R., and Woodruff, W. (2002) Direct infrared detection of the covalently ring linked His-Tyr structure in the active site of the heme−copper oxidases, *Biochemistry 41*, 14383−14390.
27. Michel, H. (1999) Cytochrome *c* oxidase: Catalytic cycle and mechanisms of proton pumping−A discussion, *Biochemistry 38*, 15129−15140.
28. Zaslavsky, D., and Gennis, R. (2000) Proton pumping by cytochrome oxidase: Progress, problems, and postulates, *Biochim. Biophys. Acta 1458*, 164−179.
29. Buse, G., Soulimane, T., Dewor, M., Meyer, H. E., and Bluggel, M. (1999) Evidence for a copper-coordinated histidine-tyrosine cross-link in the active site of cytochrome oxidase, *Protein Sci. 8*, 985−990.
30. Rogers, M., and Dooley, D. (2001) Posttranslationally modified tyrosines from galactose oxidase and cytochrome *c* oxidase, *Adv. Protein Chem. 58*, 387−436.
31. Das, T., Pecoraro, C., Tomson, F., Gennis, R., and Rousseau, D. (1998) The post-translational modification in cytochrome *c* oxidase is required to establish a functional environment of the catalytic site, *Biochemistry 37*, 14471−14476.
32. Pinakoulaki, E., Pfitzner, U., Ludwig, B., and Varotsis, C. (2002) The role of the cross-link His-Tyr in the functional properties of the binuclear center in cytochrome *c* oxidase, *J. Biol. Chem. 277*, 13563−13568.
33. Knappe, J., and Wagner, A. (2001) Stable glycyl radical from pyruvate formate-lyase and ribonucleotide reductase (III), *Adv. Protein Chem. 58*, 277−315.
34. Urbani, A., Gemeinhardt, S., Warne, A., and Saraste, M. (2001) Properties of the detergent solubilised cytochrome *c* oxidase (cytochrome cbb_3) purified from *Pseudomonas stutzeri*, *FEBS Lett. 508*, 29−35.
35. Subramaniam, S. (1998) The biology workbench−A seamless database and analysis environment for the biologist, *Proteins 32*, 1−2.
36. http://www.ncbi.nlm.nih.gov.
37. http://www.tigr.org.
38. http://www.jgi.doe.gov/JGI_microbial/html/index.html.
39. http://www.genomesonline.org.
40. Thompson, J., Higgins, D., and Gibson, T. (1994) CLUSTAL W: Improving the sensitivity of progressive multiple sequence alignment through sequence weighting, position-specific gap penalties, and weight matrix choice, *Nucleic Acids Res. 22*, 4673−4680.
41. Milpetz, F., Argos, P., and Persson, B. (1995) TMAP: A new email and WWW service for membrane−protein structural predictions, *Trends Biochem. Sci. 20*, 204−205.
42. Altschul, S., Madden, T., Schaffer, A., Zhang, J., Zhang, Z., Miller, W., and Lipman, D. (1997) Gapped BLAST and PSI−BLAST: A new generation of protein database search programs, *Nucleic Acids Res. 25*, 3389−3402.
43. Bernstein, F., Koetzle, T., Williams, G., Meyer, E. F., J., Brice, M., Rodgers, J., Kennard, O., Shimanouchi, T., and Tasumi, M. (1977) The Protein Data Bank: A computer-based archival file for macromolecular structures, *J. Mol. Biol. 112*, 535−542.
44. Guex, N., and Peitsch, M. (1997) SWISS-MODEL and the Swiss-PdbViewer: An environment for comparative protein modeling, *Electrophoresis 18*, 2714−2723.
45. Peitsch, M. (1996) ProMod and Swiss-Model: Internet-based tools for automated comparative protein modelling, *Biochem. Soc. Trans. 24*, 274−279.
46. Zhang, L., and Hermans, J. (1996) Hydrophilicity of cavities in proteins, *Proteins 24*, 433−438.
47. Kale, L., Skeel, R., Bhandarkar, M., Brunner, R., Gursoy, A., Krawetz, N., Phillips, J., Shinozaki, A., Varadarajan, K., and Schulten, K. (1999) NAMD2: Greater scalability for parallel molecular dynamics, *J. Comput. Phys. 151*, 283−312.
48. Foloppe, N., and MacKerell, J. A. D. (2000) All-atom empirical force field for nucleic acids: I. Parameter optimization based on small molecule and condensed phase macromolecular target data, *J. Comput. Chem. 21*, 86−104.
49. Szabo, A., and Ostlund, N. (1982) *Modern Quantum Chemistry: Introduction to Advanced Electronic Structure Theory*, McGraw-Hill, New York.
50. Becke, A. (1993) Density-functional thermochemistry. III. The role of exact exchange, *J. Chem. Phys. 98*, 5648−5662.
51. Hay, P. J., and Wadt, W. R. (1985) *Ab initio* effective core potentials for molecular calculations. Potentials for the transition metal atoms Sc to Hg, *J. Chem. Phys. 82*, 270−283.
52. Hehre, W. J., Ditchfield, R., and Pople, J. A. (1972) Self-consistent molecular orbital methods. XII. Further extensions of Gaussian-type basis sets for use in molecular orbital studies of organic moecules, *J. Chem. Phys. 56*, 2257−2261.
53. Michel, H. in *Biological Electron-Transfer Chains: Genetics, Composition and Mode of Operation*, p 279.
54. Todd, A., Orengo, C., and Thornton, J. (2002) Plasticity of enzyme active sites, *Trends Biochem. Sci. 27*, 419−426.
55. Todd, A., Orengo, C., and Thornton, J. (2001) Evolution of function in protein superfamilies, from a structural perspective, *J. Mol. Biol. 307*, 1113−1143.
56. Hasson, M., Schlichting, I., Moulai, J., Taylor, K., Barrett, W., Kenyon, G., Babbitt, P., Gerlt, J., Petsko, G., and Ringe, D. (1998) Evolution of an enzyme active site: The structure of a new crystal form of muconate lactonizing enzyme compared with mandelate racemase and enolase, *Proc. Natl. Acad. Sci. U.S.A. 95*, 10396−10401.
57. Branden, M., Sigurdson, H., Namslauer, A., Gennis, R., Adelroth, P., and Brzezinski, P. (2001) On the role of the K-proton-transfer pathway in cytochrome *c* oxidase, *Proc. Natl. Acad. Sci. U.S.A. 98*, 5013−5018.
58. Humphrey, W. F., Dalke, A., and Schulten, K. (1996) VMD: Visual molecular dynamics, *J. Mol. Graphics 14*, 33−38.

BI050464F